Maximum Torque Density Limit for Surface-Cooled SPM Machines

Andrea Bocchese, Jonas Kristiansen Nøland, Nicola Bianchi, Børge Noddeland and Astrid Røkke

***Abstract*—The aim of this work is to find the maximum torque density limit of a surface cooled SPM machine. In this paper, an analytical and a FEM-based model are developed under some theoretical conditions. Both models consist of a magnetic and a thermal part, where they are used to calculate the torque and the temperature distribution, respectively. Each model is then combined with an optimization process in order to maximize the torque density. The analytical model utilizes the GlobalSearch algorithm (GSA), while the FEM-based one uses the Pattern-Search (PS) approach. A case configuration is selected, and the results between the two models are presented and compared. It is shown that it is possible to determine a maximum limit for the torque density of a machine and the configuration used to get it. A parametric sensitivity analysis is carried out to analyze the influence of some typical parameters on the maximum torque density. Finally, this maximum limit is compared against typical SPMs.**

***Index Terms*—Optimization, permanent magnet machines, SPM, torque density.**

I. Introduction

The torque density is a good indicator of the performance of an electrical machine because it relates the torque to the entire volume occupied by the machine itself. Many studies have been done on performance optimization and maximization, especially in relation with power density [1], [2]. This paper focuses on the torque density barrier, achieved under strong theoretical conditions, for a classical surface-mounted permanent magnet (SPM) machine. Several different cooling strategies can be adopted nowadays [3] and they strongly affect design and performance of an electrical machine. In order to reduce the scope, this study focuses on a surface cooled SPM machine, so the cooling is limited to the selected configuration.

Usually, analytical models are utilized to formulate dimensional goodness factors for design evaluations [4]. This paper combines an analytical model along with a finite element (FE) based model for both the thermal and magnetic aspects of the SPM machine. The first gives predictions relying on strong and known formulations about electrical machines; while the second calculates the results by using FEA, as often done in this field. The interest of this work is to see what is theoretically achievable by identifying a maximum limit for the torque density, which can give some indications on where actual technologies are nowadays.

A. Bocchese, B. Noddeland and A. Røkke are with Rolls-Royce Electrical Norway, Trondheim, Norway (email: andrea.bocchese@outlook.com).

J. K. Nøland is with the Department of Electric Power Engineering, Norwegian University of Science and Technology, Trondheim, Norway.

N. Bianchi is with the Department of Electrical Engineering, University of Padova, Padova, Italy.

The remainder of the paper is organized as follows. In Section II, the design problem is clearly formulated. Then, Section III presents the analytical model before Section IV describes the FE-based model. Finally, Sections V, VI and VII present the model validation, the main results and the conclusions, respectively.

II. Problem Formulation

The goal of this paper is to find the maximum torque density limit for a surface cooled SPM machine with radial flux. In order to do that, the best-case scenario has to be considered, so for that reason, some assumptions and conditions are introduced.

1) For simplicity, the selected machine has slots with a rectangular cross-section. 2) Each slot has a single conductor. 3) There is a generic insulation layer around every single conductor. 4) The air gap clearance is almost zero. 5) The permanent magnet material is ideal, temperature-insensitive (20°C) and made of NdFeB. 6) Thermal calculations are limited to the stator only with thermal insulation between rotor and stator. 7) The machine is cooled at the outer stator surface with infinite superior cooling condition. 8) Only radial and circumferential fluxes are taken into account, not the axial ones (i.e., end-windings are not considered). 9) Other parameters, such as PM width, fill and stacking factors, are set equal to unity.

A. Torque formulation

The torque is usually derived from the Lorentz force and it is well-known that the shear stress is related to it as expressed in [5]

$$T = F\frac{D}{2} = \sigma \cdot Area \cdot \frac{D}{2}, \tag{1}$$

where σ is the shear stress (i.e., the product of magnetic flux density with linear current density), D is the diameter at the air-gap and $Area$ is equal to $\pi D L_s$. Eq. (1) shows that the torque depends mainly on the product of the magnetic loading B and the electric loading K. For this reason, each model is divided into a magnetic and a thermal part; The first one is used to calculate the torque directly, the second one acts on the linear current density by evaluating the temperature distribution. In order to maximize the torque, an optimization problem must be formulated. The variables of optimization must be properly selected.

B. Optimization problem

The optimization procedure must divide the machine into two directions; The radial and circumferential. In the radial direction, there are the rotor yoke height h_{yr}, the magnet thickness l_m, the air-gap length g, the slot height h_s and the stator yoke height h_{ys}. For the sake of simplicity, it is possible to assume that the two yoke heights are equal. In addition, the outer stator and inner rotor diameters, respectively D_{os} and D_{ir}, and the air-gap are fixed. Finally, there are four quantities varying, which means that three of them are needed while the fourth one can be derived by subtraction from the others. In the circumferential direction instead, the widths of the slot and of the tooth repeat for each slot pitch, so it is just needed to select one of the two. The geometrical variables selected are then: the magnet thickness, the slot height and the slot width. Generally, the variables are also scaled in order to work with adimensional quantities. For this reason, the variables in the circumferential direction are scaled with τ_s, while the ones in the radial direction with R_{free}, which is the part of the radius of the machine that is free to be used by the optimization process:

$$R_{free} = h_{yr} + l_m + h_s + h_{ys} = 2h_y + l_m + h_s \qquad (2)$$

Fig. 1 shows the quantities discussed and R_{free}, which is marked with a red line.

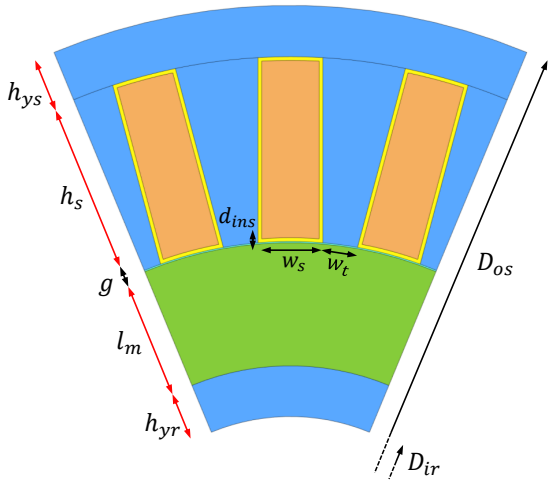

Fig. 1. SPM machine model with geometrical quantities

Furthermore, the current density $J_{s_{rms}}$ needs to be selected as an additional variable, in order to take into account the temperature limitation that is acting on the maximum value of current inside the conductors. The variables of optimization are depicted in Tab. I. A general scheme of the entire optimization process is shown in Fig. 2. First, a main script defines and elaborates all the input data and settings needed by the optimization algorithm. Then, a magnetic model calculates the objective function (i.e., the torque density), while a thermal model predicts the hot-spot temperature in the slot, which is limited by a constraint. These quantities are processed by the optimization algorithm, which after multiple iterations finds the optimum.

TABLE I
OPTIMIZATION VARIABLES

No.	Description	Variable	Relation
#1	Magnet thickness ratio	γ_{l_m}	l_m/R_{free}
#2	Slot height ratio	γ_{h_s}	h_s/R_{free}
#3	Slot width ratio	γ_{w_s}	w_s/τ_s
#4	Current density	$J_{s,rms}$	$I_{s,rms}/A_s$

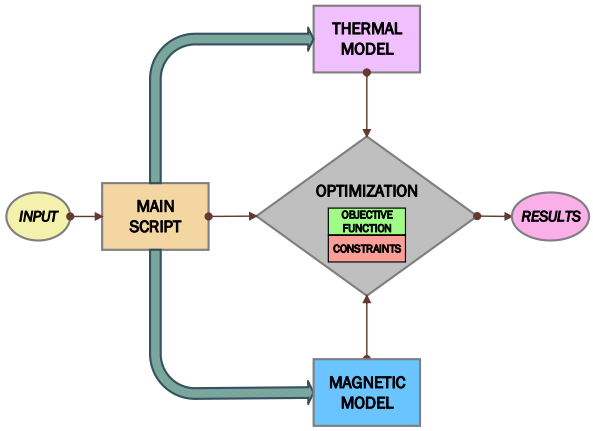

Fig. 2. Conceptual scheme of the optimization process

III. Analytical Model

This section describes the analytical model to predict the torque density limit of this type of SPMs.

A. Analytic formulation of the magnetic behaviour

The magnetic model predicts the air-gap flux density, which is needed for the torque calculation. As expressed in [6], the average air-gap flux density due to the magnet alone is

$$B_{g0} = \frac{B_r}{1 + \frac{\mu_r g}{lm}}, \qquad (3)$$

where B_r is the PM remanent flux density, μ_r is the relative permeability of the magnet and l_m is the PM thickness. The length of the air-gap, g, is previously multiplied by the Carter coefficient suggested in [7], in order to take into account the slotting effect.

Besides the magnet characteristics, another element to take into account is the saturation effect. In fact, to obtain the highest torque, in the machine there will be really high values of flux density, as also verified by FEM simulations. In this condition, the teeth and the yoke start to saturate, causing an MMF-drop and consequently increasing their reluctances. As introduced in [8], it is possible to compensate this effect by introducing an extra air-gap, that will be added to the previous Carter corrected one, which represents the reluctances:

$$g_{extra} = \mu_0 \Re_{tot} \tau_s L_s \qquad (4)$$

where $\Re_{tot}$ is the sum of the parallel-connected teeth and the stator yoke reluctances, τ_s is the slot pitch and L_s is the stator length. The tooth and stator yoke reluctance expressions used in the model, are based on the ones presented in [8], [9] and [10]. Since the saturation effect depends on the BH curve of the lamination chosen, an approximated function is used to simulate its behaviour, as explained in [9]:

$$H = a_0 B + a_1 B^n \tag{5}$$

where a_0 and a_1 coefficients are obtained by a curve fitting operation. It is possible to integrate this dependence inside of the reluctance expressions, by substituting the H/B ratio with the one derived from this function. Then to consider the saturation effect on B_{g0}, it is possible to use an iterative system with multiple iterations: it starts from values of flux density in teeth and yoke which are not considering the extra air-gap; then, for each iteration, the reluctances are calculated, the corrected air-gap length is obtained and used to get the new B_{g0}, from which the new flux densities B_t and B_{ys} are derived. Finally, a new iteration starts with these new values. In each iteration, B_t and B_{ys} are calculated as explained respectively in [8] and [10]. In the end, the rms value of the fundamental space component of the air-gap flux density B_{1g} is obtained, so the torque can be calculated as expressed in [6]:

$$T = 2\pi(\frac{D_{is}}{2})^2 L_s B_{1g} K_{1s} \sin\beta \tag{6}$$

where K_{1s} is the rms value of the linear current density, and β is the angle between the fields generated by the magnet and by the stator current, which is taken equal to 90° to have the maximum torque.

B. Lumped thermal network modeling

The thermal part of the model calculates the temperature distribution in the stator. It predicts the value of the hot spots inside the slots (i.e., evident from the assumptions made). In this way, it is possible to put a limit on the linear current density (for the torque calculation) from the maximum allowable temperature in the insulation as a constraint. The rms linear current density is defined as the total current on all the conductors divided by the entire inner stator circumference:

$$K_{1s} = \frac{I_{s_{tot}}}{\pi D_{is}} \tag{7}$$

where $I_{s_{tot}}$ is calculated by multiplying the rms current density $J_{s_{rms}}$ with the conductor cross-section for each slot. A thermal lumped circuit for the stator using arc-segment elements is created, following the modeling procedure explained in [11]. Since only radial and circumferential heat fluxes are taken into account, each element is composed of two T-structures linked to a central node. Only a slot pitch representation is needed because the same configuration repeats along the stator. Firstly an extended circuit is composed, then the several thermal resistances are aggregated in order to get a reduced model, which is finally used to compose the thermal conductance matrix $[G]$. So the final network consists of 5 nodes, respectively one for the slot, one for the tooth, two for the yoke and one for the outer surface, as shown in Fig. 3. The points in red and yellow are heat source nodes, while the blue one is where is applied the cooling condition.

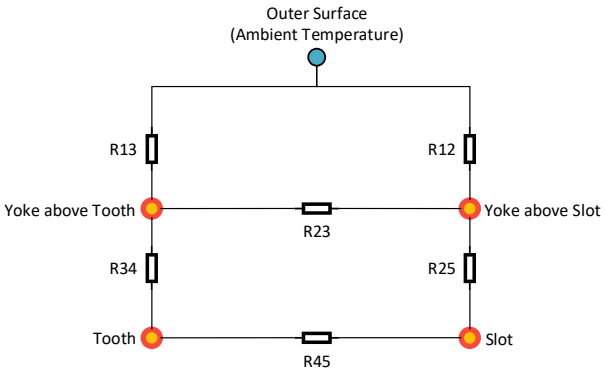

Fig. 3. Reduced Thermal Network

The infinite superior cooling condition assumed in the outer surface is practically fixing its temperature to the one of the ambient, which is set to 20°C in this study.

Regarding the losses vector $[P]$, both Joule and iron ones need to be considered. The Joule losses are simply calculated as follows:

$$P_{cu} = \rho_{T_{max}} J_{s_{rms}}^2 A_{coil} Q_s \tag{8}$$

where $\rho_{T_{max}}$ is the resistivity at the maximum temperature reachable , A_{coil} is the conductor cross-section and Q_s is the number of slots. The iron losses are calculated using the Steinmetz's equation reported in [7], by multiplying the specific losses found by the weight of teeth and yoke respectively. Finally the temperature distribution is calculated by the product of the losses vector and the inverse of the thermal conductance matrix:

$$[T] = [G]^{-1}[P] \tag{9}$$

C. Optimization Process

The optimization process follows the main aspects introduced in the first section. The optimization algorithm used for the analytical model is the GlobalSearch (GS). A maximum number of iterations and function evaluations is set, as safety against divergence. The solver run by the GlobalSearch is *fmincon*, with an interior-point algorithm. The boundaries selected are shown in Tab. II.

TABLE II
CONSTRAINTS ON OPTIMIZATION VARIABLES

Bounds	**Variables of Optimization**			
	γl_m	γh_s	γw_s	$J_{s_{rms}}$
Lower	0.01	0.01	0.01	0.01
Upper	1	1	1	50

Inequality and equality constraints are also selected. The first ones:

- γ_{l_m}, γ_{h_s}, γ_{w_t} and γ_{w_s} are set to be positive
- $\gamma_{h_{ys}}$ and $\gamma_{h_{yr}}$ are set to be higher than 0.01, to not become zero
- all the temperatures calculated ($T_{yoke_{tooth}}$, $T_{yoke_{slot}}$, T_{tooth}, T_{slot}) are set to be positive and less than the maximum allowable temperature

The second ones:

- the sum of γ_{l_m}, γ_{h_s}, $\gamma_{h_{ys}}$ and $\gamma_{h_{yr}}$ is set to be equal to 1
- the sum of γ_{w_s} and γ_{w_t} is set be equal to 1

IV. FEM-BASED MODEL

The FEM-based model consists of two types of simulation, magnetic and thermal. So, two separated models are created in order to simulate the machine. To do that, some indications expressed in [12] are used. The simulations are at steady state and the geometry is 2D.

A. Magnetic Part

For the magnetic part, only a pole pitch representation is needed for the calculation of the torque. Doing this, the computational cost of the simulation decreases. Since the optimization will modify the geometry during the process, a particular attention must be given to its creation, to avoid problems as unwanted domains and geometry violations. Regarding the physics, a *Magnetic Insulation* condition is applied to the outer and inner arc-segments, respectively of the stator and rotor yokes. Moreover, an *Anti-periodicity* is applied to the lateral boundary lines of the pole-section on study. Different relations are applied to each type of material; for air and insulation, their relative permeability is assigned. For iron domains, the B-H curve constitutive relation is adopted:

$$B = f(|H|)\frac{H}{|H|} \tag{10}$$

On the permanent magnet domain, its remanent flux density is used:

$$B = \mu_0 \mu_r H + B_r \tag{11}$$

Regarding the copper domains, a current is assigned for each phase:

- Phase A: $I_{peak}\cos(\theta)$
- Phase B: $-I_{peak}\cos\left(\theta - \frac{2\pi}{3}\right)$
- Phase C: $-I_{peak}\cos\left(\theta - \frac{4\pi}{3}\right)$

where $\theta = 0$ in this case, in order to have the maximum value for the torque, and the negative sign for the two phases (B,C) is to take into account the opposite direction of the current in those two conductors. Finally, the torque is calculated by using the Maxwell's Stress Tensor around the rotor. Fig. 4 shows an example of the model created.

B. Thermal Part

For the thermal part, only a slot pitch representation is needed in order to evaluate correctly the temperature on the stator. So in this case, the geometry is showing simply a slot, half of each adjacent tooth and the yoke above them. Regarding the physics, a *Thermal Insulation* condition is applied to all the external boundaries, so that the heat flux does not cross them, except on the outer surface. In fact, here it is applied a convective heat flux:

$$q_0 = h \cdot (T_{ext} - T) \tag{12}$$

where h is the heat transfer coefficient and T_{ext} is the external temperature, which is taken equal to the ambient temperature (in K). Regarding the heat transfer coefficient, in order to have the infinite superior cooling, it is chosen a really high value: $h = 1 \cdot 10^9 \ \frac{W}{m^2 K}$. Assigning a fixed temperature on that boundary, would be equivalent. Heat sources are assigned to the conductor and iron domains. On the first, a volumetric heat source is defined by using the following formula:

$$Q_0 = \rho_{T_{max}} J^2_{s_{rms}} \tag{13}$$

Regarding the iron losses, as done before, they are defined analytically by using the Steinmetz's equation both for the two half-tooth and the yoke. Finally, the temperature distribution is evaluated and the maximum value reached is extracted and processed in the optimization. Fig. 5 shows an example of the model created.

C. Optimization Process

The optimization algorithm used in this case is the Pattern-Search, a direct search method. As done before, a maximum number of iterations and function evaluations is set. Moreover a complete poll is done at each iteration in the mesh searching points of the algorithm. In addition, a maximum time is selected in order to speed up the entire optimization process. If not, a lot of time would be wasted to reach an accuracy not needed on the variables and solution. Generally the maximum time selected is $5400 - 7200\ s$, for each γ_D point studied. The boundaries selected in this case are different from the ones used for the analytical model. The search domain is reduced in accordance to the results of the other optimization, in order to help the algorithm. More in particular, the bounds for the current density $J_{s_{rms}}$ are chosen around the same order of magnitude given from the other optimization. It could happen that the algorithm selects an infeasible value for the variables, which is violating the geometric constraints, causing a problem in the geometry construction. To avoid this situation, an *if/else* command is used in the scripts of both the magnetic and thermal parts as a checking point. More in particular, in these situations, the geometry is not updated and an almost-zero torque and a really high temperature are taken as results of that iteration. This additional command is not really affecting the performance of the optimization and it helps to prevent a stop on the FE analysis.

Regarding the inequality constraints:

- γ_{l_m}, γ_{h_s}, $\gamma_{h_{ys}}$, $\gamma_{h_{yr}}$ γ_{w_t} and γ_{w_s} are set to be higher than 0.01, to not become zero
- $T_{max_{reached}}$ is set to be positive and less than the maximum allowable temperature

In addition, if the temperature $T_{max_{reached}}$ is too much lower than the limit chosen, that iteration is discarded and the torque

evaluation is not done. This helps to speed up the process. Regarding the equality constraints:

- the sum of γ_{l_m}, γ_{h_s}, $\gamma_{h_{ys}}$ and $\gamma_{h_{yr}}$ is set to be equal to 1
- the sum of γ_{w_s} and γ_{w_t} is set be equal to 1

V. Verification

Firstly the two models are verified by comparing the torque and the temperatures obtained without the optimization process. In Tab. III some general input data used in this test are shown.

TABLE III
Test General Input Data

D_{os}	500.00 mm		$J_{s_{rms}}$	8.5 A/mm^2
D_{ir}	200.00 mm	$(\gamma_D = 2.5)$	d_{ins}	0.50 mm
L_s	500.00 mm	$(\gamma_L = 1)$	B_r	1.4 T
g	0.05 mm		α	1
l_m	44.97 mm	$(\gamma_{l_m} = 0.3)$	μ_r	1.05
h_s	44.97 mm	$(\gamma_{h_s} = 0.3)$	q	1
h_y	29.98 mm	$(\gamma_{h_y} = 0.2)$	m	3
w_s	22.90 mm	$(\gamma_{w_s} = 0.5)$	P	8
w_t	22.90 mm	$(\gamma_{w_t} = 0.5)$	f	50 Hz

In Tab. IV are also shown the data about the materials, used mainly in the thermal part.

TABLE IV
Test Material Data

k_{coil}	400 W/(m · K)		K_{hy}	0.84 W/kg	$(70\% \cdot K)$
k_{fe}	30 $W/(m \cdot K)$		K_{ec}	0.36 W/kg	$(30\% \cdot K)$
k_{iso}	0.2 $W/(m \cdot K)$		B_o	1 T	
T_{amb}	20 $°C$		f_0	50 Hz	

The results are presented in Tab. V and show that the two models are working similarly, with minor differences. Figures 4-5 show respectively the magnetic and thermal configurations obtained for the test done.

TABLE V
Test Results

Description	Analytical	Finite element
Torque	18390 Nm	17725 Nm
Volume	0.098175 m^3	0.098175 m^3
Torque/Volume	$1.8731 \cdot 10^5$ N/m^2	$1.8054 \cdot 10^5$ N/m^2
Slot Temperature	104.94 $°C$	104.1 $°C$
Tooth Temperature	73.15 $°C$	72.9 $°C$
Yoke Temperature	38.2 $°C$	37 $°C$

VI. Results

A. Study for a Selected Configuration

Once tested the two models separately, the optimization can be done. First of all, a configuration is selected to compare the optimization of the two models and see how the two algorithms actually work. The configuration selected is shown in Tab. VI. Regarding the material data, they are the same used in Tab. IV.

What is found in this study is a line - which in fact describes the torque density limit - to varying of the ratio of the outer stator diameter to the inner rotor one, which is defined as γ_D. Figures 6-7 show respectively the results obtained for the analytical and FEM-based model, with the iterations done by the algorithm and three magnetic configurations, as graphical feed-backs. Comparing Fig. 6-7, it is possible to see that the analytical predictions and the FE results have a similar trend and order of magnitude, with minor differences: mostly about 2-3%, while around 6% in the worst point. More in particular, observing all the iterations done by the two algorithms, it can be seen the difference between them: the GlobalSearch finds the optimum by starting from multiple points and sometimes it can violate the constraints, but discarding those points; instead, the Pattern-Search used in combination with the *if/else* command, finds the optimum by getting closer step by step without violating the constraints. In addition, in Fig. 8 is shown

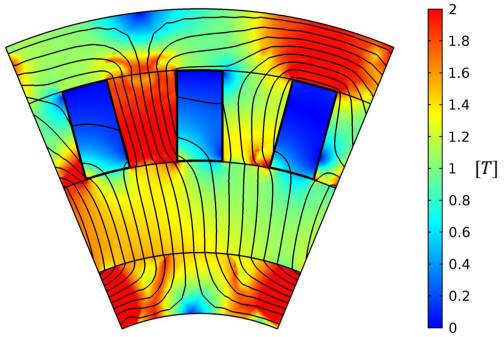

Fig. 4. Static flux map of the loaded SPM under torque verification. Magnetic flux density values in [T].

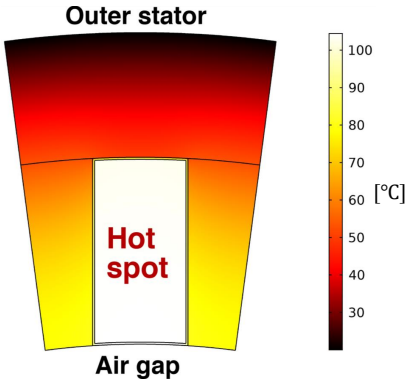

Fig. 5. Temperature footprint along the stator (one slot width) under thermal verification. Temperature values in [°C].

TABLE VI
General Input Data for the Configuration Selected

D_{os}	200 mm		q	1
L_s	200 mm	$(\gamma_L = 1)$	m	3
g	0.05 mm		f	50 Hz
d_{ins}	0.2 mm		B_r	1.4 T
$T_{max_{ins}}$	220 °C	(Class C)	μ_r	1.05
P	8		α	1

a comparison between the final variables of optimization found.

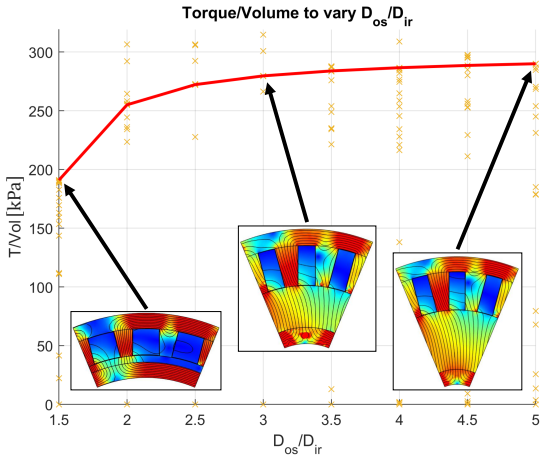

Fig. 6. Configuration Selected: Torque/Volume to vary D_{os}/D_{ir} obtained from the analytical model.

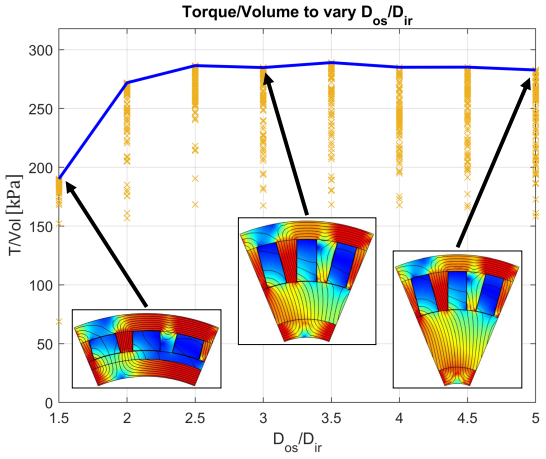

Fig. 7. Configuration Selected: Torque/Volume to vary D_{os}/D_{ir} obtained from the FEM-based model.

B. Parametric Sensitivity Analysis of Torque Density

Finally, a sensitivity analysis is done to investigate the influence on the torque density limit of some typical parameters, such as insulation thickness, number of poles, air-gap length and insulation class. Other parameters remain the same in all these studies: $D_{os} = 500\ mm$, $L_s = 500\ mm$, $q = 1$ (slots per phase per pole), $m = 3$ (number of phases), $f = 50\ Hz$, $B_r = 1.4\ T$, $\mu_r = 1.05$ and $\alpha = 1$. The material data used is the same introduced in Tab. IV

The first analysis is done for the variation of the insulation thickness $d_{ins} = 0.2/0.5/1\ mm$. They correspond to three voltage levels, which are respectively 500 V, 1.25 kV and 2.5 kV (considering the typical value of 2.5 kV/mm from literature). Other parameters, previously not declared, are now equal to: $g = 0.05\ mm$, $T_{max_{ins}} = 180\ °C$ (class H), $P = 8$ (number of poles). Fig. 9a) shows the results for the variation

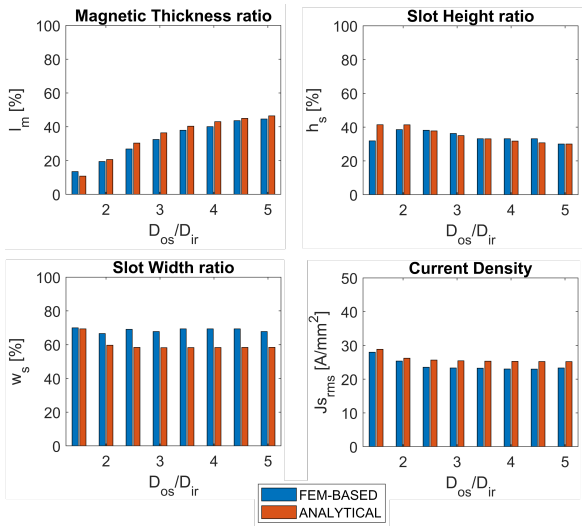

Fig. 8. Configuration Selected: histogram comparison for the variables of optimization.

of d_{ins} and, as expected, for an higher value the torque density decreases. More in particular, taking the curve for $d_{ins} = 0.2$ mm as reference, the drop is about 18-20% for $d_{ins} = 0.5$ mm and about 32-36% for $d_{ins} = 1\ mm$.

The second analysis is done for the variation of the insulation class F/H/C, which correspond to a maximum temperature allowable $T_{max_{ins}} = 155/180/220\ °C$. Other parameters, previously not declared, are now equal to: $g = 0.05\ mm$, $P = 8$, $d_{ins} = 0.2\ mm$. Fig. 9b) shows the results for different classes of insulation. As expected, using a better insulation class results in a higher value of torque density. More in particular, taking as reference the curve for class C, the best one considered, the drop is about 6-7% for class H and about 12% for class F. More in general, other information related to temperature sensitivity can also be deduced from this analysis.

The third analysis is done for the variation of the number of poles $P = 4/8/12$, considering the same number of slots per pole per phase. Other parameters, previously not declared, are now equal to: $g = 0.1\ mm$, $T_{max_{ins}} = 220\ °C$ (class C), $d_{ins} = 0.5\ mm$. Fig. 9c) shows the results for the variation of the number of poles. For machines with an higher value of P, the torque density increases. This is intuitive, since having a fixed q, if the number of poles increases also the number of slots does. More in particular, taking the curve for $P = 12$ as reference, the drop is about 14-20% for $P = 8$ and about 42-47% for $P = 4$. Moreover, the drop between two consecutive curves is lower for higher values of P.

The fourth analysis is done for the variation of $g = 0.05/0.5/1/1.5\ mm$. Other parameters, previously not declared, are now equal to: $P = 8$, $T_{max_{ins}} = 220\ °C$ (class C), $d_{ins} = 0.5\ mm$. Fig. 9d) shows the results for the variation of the air-gap length. As can be noticed, g does not have a big influence on the torque density, also due to the presence of a thermal insulation between rotor and stator.

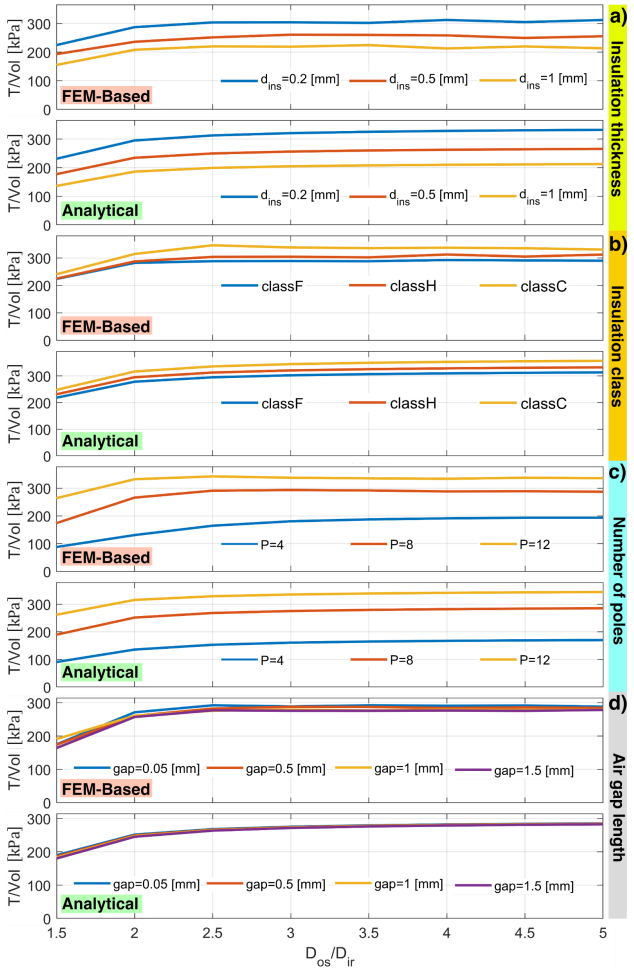

Fig. 9. Sensitivity to torque density. **a)** Insulation thickness. **b)** Insulation class. **c)** Number of poles. **d)** Air gap length.

VII. Conclusions

This paper determines the maximum torque density limit for an SPM machine, as well as indicating the topology needed to get it. For the sake of comparability, some typical values of the air-gap torque of electrical machines should be considered. Conventional machines with a similar size as the case study have shear stress of about $20 - 35\ kPa$. The results obtained show that the classical benchmark values are only a fraction of the maximum limit found (i.e., about one-tenth). For larger machines, the limit moves up, but the typical values get closer to it, thanks to a better cooling system generally adopted in those machines. It underlines the importance of thermal aspects.

It can be seen from the trends that a stretched machine (low value of D_{os}/D_{ir}) leaves more space to the slots and the yokes, presumably due to the presence of a high saturation in iron. Consequently, for higher values of that ratio, it seems beneficial to employ a bigger PM thickness. It is worth nothing that such considerations are not accounting for the practical design issues, as the economic aspects are neglected.

The parametric sensitivity analysis pointed out the importance of the insulation in the design of an electrical machine. Another important aspect to consider is the number of poles, considering a fixed q. Moreover, the air-gap length has proven to be not that sensitive, when focusing on the magnetic aspects.

In conclusion, since some strong assumptions and conditions were selected in order to identify this limit, a further step could be to reduce some of them to get closer to reality and to evaluate their implications on the limit found. In addition, future studies could try to apply this methodology to other types of machine.

References

[1] F. Cupertino, R. Leuzzi, V. G. Monopoli, and G. L. Cascella, "Maximisation of power density in permanent magnet machines with the aid of optimisation algorithms," *IET Elect. Power Appl.*, vol. 12, no. 8, pp. 1067–1074, 2018.

[2] D. Golovanov, L. Papini, D. Gerada, Z. Xu, and C. Gerada, "Multidomain optimization of high-power-density pm electrical machines for system architecture selection," *IEEE Trans. Ind. Electron.*, vol. 65, no. 7, pp. 5302–5312, July 2018.

[3] M. Popescu, D. A. Staton, A. Boglietti, A. Cavagnino, D. Hawkins, and J. Goss, "Modern heat extraction systems for power traction machines—a review," *IEEE Transactions on Industry Applications*, vol. 52, no. 3, pp. 2167–2175, 2016.

[4] S. G. Lee, J. Bae, and W. Kim, "A study on the maximum flux linkage and the goodness factor for the spoke-type pmsm," *IEEE Trans. Appl. Supercond.*, vol. 28, no. 3, pp. 1–5, April 2018.

[5] W. Soong, "Sizing of electrical machines," *Power Eng. Briefing Note Series*, vol. 9, pp. 17–18, 2008.

[6] G. R. Slemon, "On the design of high-performance surface-mounted pm motors," *IEEE Trans. Ind. Appl.*, vol. 30, no. 1, pp. 134–140, Jan 1994.

[7] T. A. Lipo, *Introd. AC machine design*. John Wiley & Sons, 2017.

[8] P. Thelin and H. Nee, "Calculation of the airgap flux density of pm synchronous motors with buried magnets including axial leakage and teeth saturation," in *Proc. Int. Conf. Electr. Mach. Drives*, Sep. 1999, pp. 339–345.

[9] H. Polinder, J. G. Slootweg, J. C. Compter, and M. J. Hoeijmakers, "Modelling a linear pm motor including magnetic saturation," in *Proc. Int. Conf. Power Electron. Mach. Drives*, June 2002, pp. 632–637.

[10] P. Thelin and H. . Nee, "Analytical calculation of the airgap flux density of pm synchronous motors with buried magnets including axial leakage, tooth and yoke saturations," in *Proc. Int. Conf. Power Electron. Var. Speed Drives*, Sep. 2000, pp. 218–223.

[11] N. Simpson, R. Wrobel, and P. H. Mellor, "A general arc-segment element for three-dimensional thermal modeling," *IEEE Trans. Magn.*, vol. 50, no. 2, pp. 265–268, Feb 2014.

[12] N. Bianchi, *Electrical machine analysis using finite elements*. CRC press, 2017.

VIII. Biographies

Andrea Bocchese received the M.Sc. degree in electrical engineering from the University of Padova, Padova, Italy, in 2020.

Jonas Kristiansen Nøland (IEEE S'14-M'17) received the Ph.D. degree in eng. physics from Uppsala University, Uppsala, Sweden, in 2017. He is currently an Associate Professor with the Norwegian University of Science and Technology, Trondheim, Norway. Dr. Nøland is currently serving as an Editor for the IEEE TRANSACTIONS ON ENERGY CONVERSION.

Nicola Bianchi (IEEE M'98-SM'0-F'14) received the M.Sc. and Ph.D degrees in electrical engineering from the University of Padova, Padova, Italy, in 1991 and 1995, respectively. Since 2005 he has been an Associate Professor in Electrical Machines, Converters, and Drives with the Electric Drive Laboratory, Department of Electrical Engineering. He is a member of the Electric Machines Committee and the Electrical Drives Committee of the IEEE Industry Applications Society.

Børge Noddeland received the M.Sc. degree in electrical engineering from the Norwegian Univ. of Science and Technology, Trondheim, Norway, in 2007.

Astrid Røkke received the M.Sc. and Ph.D. degree in electrical engineering from the Norwegian Univ. of Science and Technology, Trondheim, Norway, in 2007 and 2017, respectively.